Sensors & Transducers, Vol. 227, Issue 11, November 2018, pp. 51-59

www.sensorsportal.com

Sensors & Transducers

Published by IFSA Publishing, S. L., 2018
http://www.sensorsportal.com

120 mV-Startup Boost Converter for Thermal Energy Harvesting System

Chun-Lian Chen and Chun Yi
Department of Electrical Engineering, National Taipei University, Taiwan
Tel.: + 886-2-86741111, fax: 886-2-26736500

Received: 31 July 2018 /Accepted: 28 September 2018 /Published: 30 November 2018

Abstract: This work presents an ultra-low startup voltage boost converter for thermal energy harvesting. The proposed architecture is composed of an LC-tank oscillator, a 3-stage charge pump and a DC to DC boost converter. A test chip is implemented in a 0.18 μmCMOS technology. The minimum input voltage is 120 mV and output voltage can achieve above 1 V. The output produces regulated 1.2 V and supplies 302 uA current for charging NiMH battery to rated voltage 1.2 V when input voltage is in range from 140 mV to 230 mV. The conversion efficiency is 34 % at minimum input voltage. A maximum efficiency of 60 % can be successfully performed. By incorporating the boost converter and a thermoelectric generator (TEG), a miniaturized module is demonstrated for energy harvesting applications.

Keywords: Boost converter, Conversion efficiency, Energy harvesting, Charge pump, Thermoelectric generator.

1. Introduction

In the past few years, a miniaturized transformer has been developed for the implementation of low-voltage DC to DC boost converter. However, the conversion efficiency is generally low for an input voltage, making it less attractive for applications. In this work, a fully electrical startup circuit is presented. We use native device to implement this circuit so it can easily operate at ultra-low voltage. Furthermore, we combine charge pump with boost converter which demonstrates a minimum input voltage of 120 mV and maximum efficiency of 34 % for thermoelectric energy harvesting applications.

The paper is organized as follows. Section 2 introduces the architecture and operation of the proposed converter. Detailed circuit implementations for each block and experimental results are presented in Sections 3 and Sections 4. Sections 5 shows layout and floor plan. Finally, a concluding remark is given in Sections 6.

2. Architecture and Circuit Design

Fig. 1 shows the block diagram of energy harvesting system, which consists of six function blocks: a LC-tank oscillator, a charge pump, a duty cycle control, a taper buffer, a boost converter and a charge control. As the input voltage V_{in} exceeds the minimum value for startup, which is approximately 120 mV, the LC-tank becomes operational and provides a pair of 300 mV pulse to charge pump, then charge pump starts to charge to 500 mV as duty cycle control's power supply. Duty cycle control is able to produce a clock which amplitude is 500 mV and duty cycle is 75 % in order to drive boost converter successfully. When boost converter startup, it can boost from ultra-low input voltage to 1.3 V output voltage to make charge control circuit normally work. Charge control circuit is like Low drop regulator (LDO), it can regulate the output voltage and additionally provide a protection mechanism to avoid battery over charging.

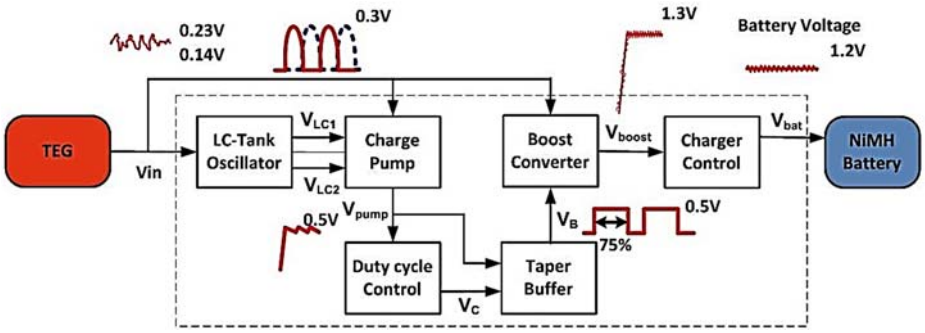


Fig. 1. Block diagram of energy harvesting system.

Finally, this chip give a fixed output voltage 1.2 V and current 300 μA to NiMH charge for storing energy.

3. Circuit Implementation

3.1. LC-Tank Oscillator

Since V_{DD} is ultra-low, charge pump needs enough high amplitude signal to charge to 0.5 V for duty cycle control. So, we use LC-Tank Oscillator. It can provide higher output amplitude $V_{DD} + \Delta V$ for charge pump. Fig. 2 shows loading equivalent LC-Tank Oscillator, C_1, C_2 for the inductance parasitic capacitor, C_C, C_L, R_L is next stage charge pump's coupled capacitor, loading capacitance, loading resistor. For operating low voltage, we use native device M_1, M_2 to cross couple to form a negative resistor. If this negative resistor is greater or equal than inductance's parasitic resistor, making oscillator produce energy is not consumed by parasitic resistor, so LC-Tank can resonates continuously to provide a stable clock signal.

3.2. All Native Differential Drive Charge Pump

There are a lot of techniques for improving charge pump in recent year. Charge pump was developed from Dickson Charge Pump which is limited by threshold voltage reduction for each device. The use of the Static Charge Transfer Switches improves output voltage to avoid threshold voltage drop by connecting gate voltage to the high voltage at the next stage, but make MOS cannot be complete turned off. Dynamic Charge Transfer Switches not only decrease the threshold voltage reduction, but also turn MOS on and off properly. However, output voltage is boosted in one of the two phases only. Differential Drive Charge Pump operates in full cycle of control signal and reduces threshold voltage drop at same time, it has more conversion efficiency in recent years. So we choose Differential Drive Charge Pump as the proposed circuit's charge pump, moreover, Fig. 3 shows the proposed charge pump, we use all native device other than NMOS or PMOS, make it be suitable for operating at low ultra-voltage. In addition to, we apply accumulation-mode MOS varactor which is higher capacitance than common MIM capacitor at low voltage. It can save chip area to reduce cost.

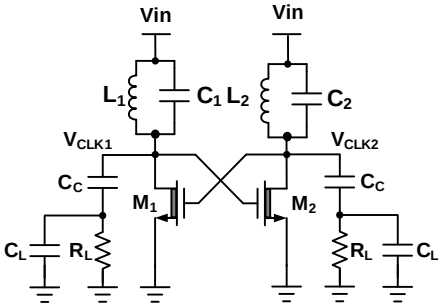


Fig. 2. Loading equivalent LC-Tank Oscillator.

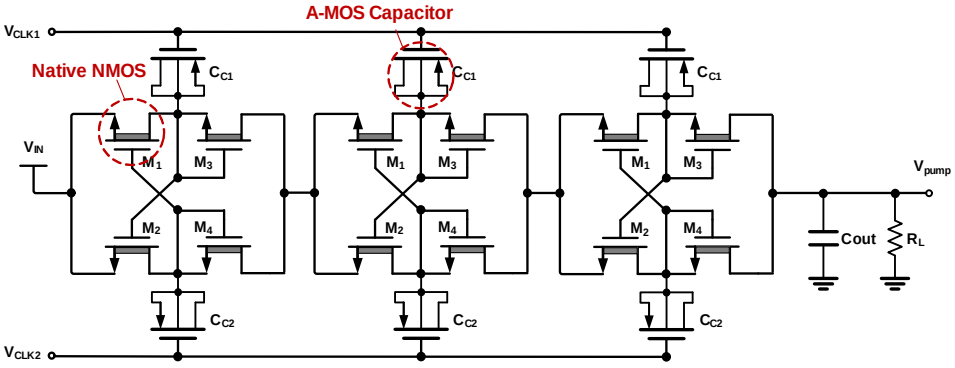


Fig. 3. All Native Differential Drive Charge Pump.

3.3. Duty Cycle Control

Fig. 4 shows a ring oscillator. First, we need a clock amplitude which is 0.45~0.55 V to control next stage boost converter's power NMOS switch only if boost converter startup successful. So, we use a simple structure ring oscillator to provide a clock for boost converter. Besides, we employ a combined logic circuit which consists of a D Flip-Flop, a NAND gate through transmission gate constituting to help boost converter rise greater output voltage. They are displayed in Fig. 5. Following, we connect D Flip-Flop's input D and inverse output Q-. It will produce a half frequency signal Q. Connecting CLK, Q, Q- to NAND gate, it adjust to turn on upper or lower transmission gate conduct input signal to provide a 75 % duty cycle for boost converter. Fig. 6 shows signal waveform.

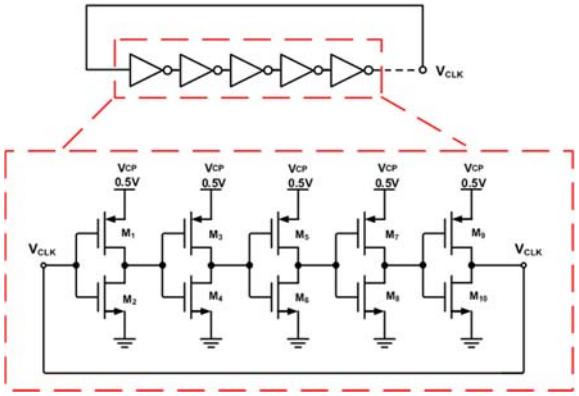


Fig. 4. Ring Oscillator.

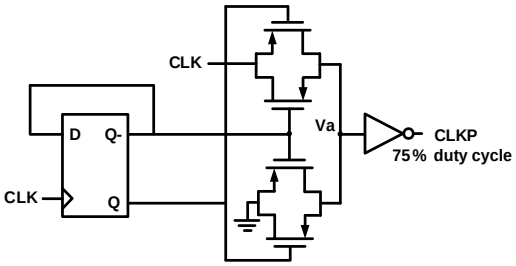


Fig. 5. D Flip-Flop and NAND gate.

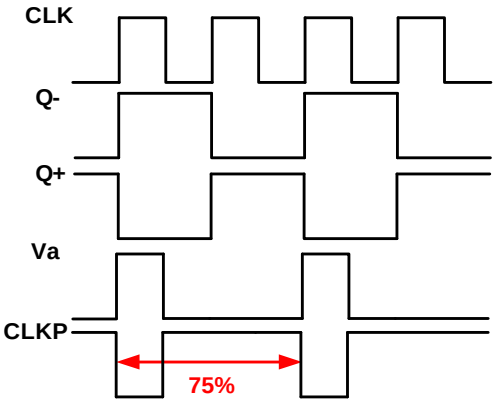


Fig. 6. Signal Waveform.

3.4. Taper Buffer

Fig. 7 shows Taper Buffer. We need to use a taper buffer to enhance its driving capability because boost converter's power MOS is large size. This circuit we simply series even stages inverter to avoid changing signal logic. Additionally, we employ dynamic threshold control technology which connects MOS's source and gate to increase output current efficiently. When NMOS turn on, NMOS's V_{BS} is high, according to body effect Formula (1). Thus, we can know that threshold voltage decreases and saturation current increases.

$$Vth = Vth0 + \gamma(\sqrt{|2\emptyset_F + V_{SB}|} - \sqrt{|2\emptyset_F|}) \qquad (1)$$

3.5. Boost Converter

Fig. 8 shows the traditional boost converter. We employ this converter as main boost circuit which is driven by previous stage providing a 75 % duty cycle clock. Additionally, we use NMOS as a power MOS because NMOS has lower threshold voltage than PMOS in process that can reduce previous stage's load. This circuit operates discontinuous conduction mode (DCM) because we need to boost to higher voltage from ultra-low input voltage. The DCM can provide a higher boost ratio and we will derive its formula in later.

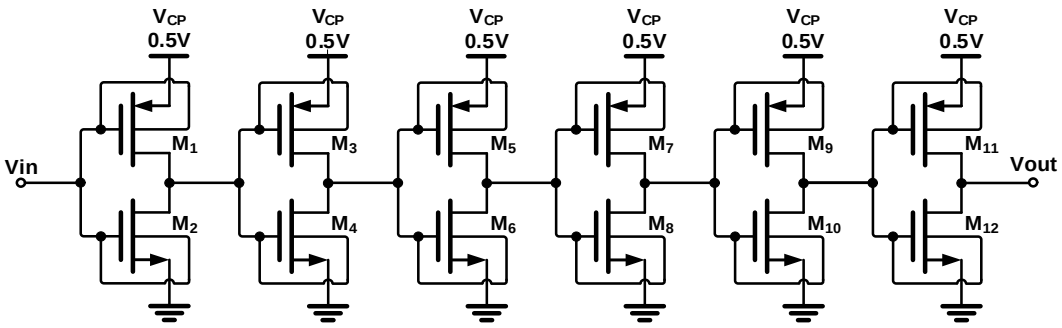


Fig. 7. Taper Buffer.

Finally, we replace diode with diode-connected NMOS to implement this converter because NMOS is easily designed and controlled.

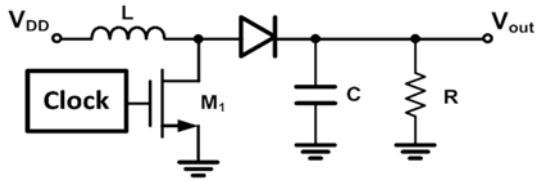


Fig. 8. Boost Converter.

Next, we introduce the principle of operation. First, in Fig. 9, you can see boost converter operates at charged period, and the inductor-current flow through the power MOS M_1 to ground. At the same time, the inductor starts to store energy.

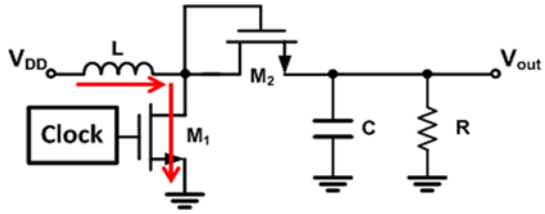


Fig. 9. Boost Converter in charged period.

The inductor-current start to increase linearly that can be calculated by using familiar relationship:

$$\Delta I_L(+) = \frac{V_L}{L} \times T_{on} = \frac{V_L}{L} \times D \times T_S \qquad (2)$$

The quantity $\Delta I_L(+)$ is the inductor ripple current, V_L is inductor-voltage, D is duty cycle, the period T_{on} is state that NMOS turn on. During this period, output load current is supplied by output capacitor C.

Fig. 10 shows that boost converter at discharged period, and the inductor-current flow through diode-connected NMOS to output load. Because inductor resists current change, it happens Lenz's law that make the inductor-voltage boost. Finally, the inductor-voltage plus V_{DD} can reach higher output voltage.

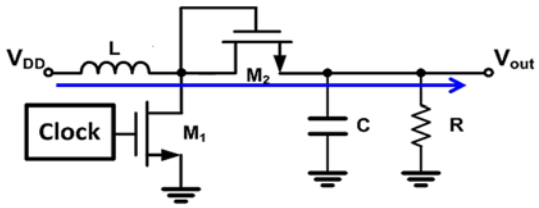


Fig. 10. Boost Converter in discharged period.

The inductor-current decrease during the NMOS off state is given by:

$$\Delta I_L(-) = \frac{V_{out} - V_{DD}}{L} \times T_{off} = \frac{V_L}{L} \times D_2 \times T_S \qquad (3)$$

The period T_{off} is the NMOS turn off period, D_2 is the complementary duty cycle D. Because $\Delta I_L(+)$ must be equal to $\Delta I_L(-)$, we can give an equation for V_{out} is:

$$V_{out} = V_{DD} \times \frac{T_{on} + T_{off}}{T_{off}} = V_{DD} \times \frac{D + D_2}{D_2} \qquad (4)$$

Now we calculate the output current which is average over the complete switching cycle of the inductor-current during the D_2 interval:

$$I_{out} = \frac{V_{out}}{R} = \frac{1}{T_S} \times [\frac{1}{2} \times (\frac{V_L}{L} \times D \times T_S) \times D_2 \times T_S] \qquad (5)$$

Then, simplifying I_{out} equation can obtain an equation for V_{out} is:

$$I_{out} = \frac{V_{out}}{R} = \frac{V_{DD} \times D \times D_2 \times T_S}{2 \times L} \qquad (6)$$

We now have two equations, one for the output current, and one for output voltage. Then solve each equation for D_2 and set the two equations equal to each other. The resulting equation can be used to derive an expression for discontinuous conduction mode output voltage V_{out} is:

$$\frac{V_{out}}{V_{in}} = 0.5 + 0.5\sqrt{1 + \frac{2D^2 R_{load} T_S}{L}} \qquad (7)$$

Thus, we can change many parameters duty cycle D, inductance L and the clock period T_S to adjust boost ratio which we need.

Next, we will introduce inductance value which we how choose. A boost converter can be designed to operate in discontinuous conduction mode (DCM) or continuous conduction mode (CCM) for load current. Thus we can calculate output current to determine inductance value. First, define output current as the minimum current to maintain continuous conduction mode, normally referred to as the critical current. It is easier to perform the derivation using the inductor current. The minimum average inductor current to maintain continuous conduction mode is given by:

$$I_{min} = \frac{\Delta I_L}{2} \qquad (8)$$

Second, calculate L such that the above relationship is satisfied. To solve the above equation, we use $\Delta I_L(+)$. The worst case condition for the boost converter is at input voltage equal to one-half of the output voltage because this gives the maximum ΔI_L. Now, we substitute and solve for L_{min}:

$$L_{min} \geq \frac{1}{2} \times V_{in} \times T_S \times D \times I_{min} \qquad (9)$$

The above equation can be simplified to shown:

$$L_{min} \geq \frac{V_{out} \times T_S}{16 \times I_{out}} \quad (10)$$

Using the inductor value which is just calculated ensures operation for output load current above the critical current. For example, if we want to operate DCM, we can select inductor value is less than L_{min} to correspond with requiring output current.

Conversion efficiency is very important for boost converter. Generally, diode-connected M_2 threshold voltage is mainly influenced factor because it will have a voltage drop which cause large power consumption. Traditional, we usually connect M_2 body with ground and its threshold voltage which is 793 mV will be very high result from body effect. Moreover, even if we connect to source to avoid body effect influenced, its threshold voltage still has 515 mV. Both threshold voltages are shown in Fig. 11. Thus, we design an improved boost convert which is displayed in Fig. 12. In this converter, we extra add a diode-connected NMOS M_3 connect original diode-connected NMOS M_2 body. While M_3 turn on, its drain voltage conduct to M_2 body then M_2 source-bulk voltage V_{SB2} will be negative that can make M_2 threshold voltage be lower. So this converter can increase conversion efficiency successfully by reducing M_2 voltage drop. Simulation is shown in Fig. 13.

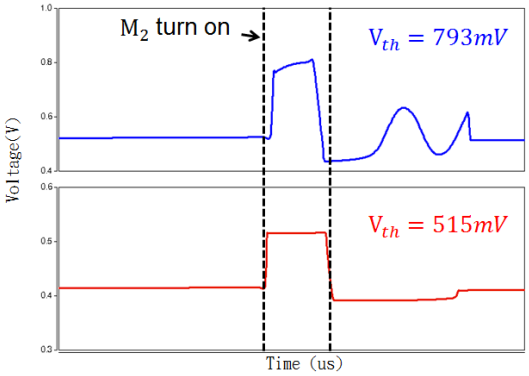


Fig. 11. Threshold voltage simulation.

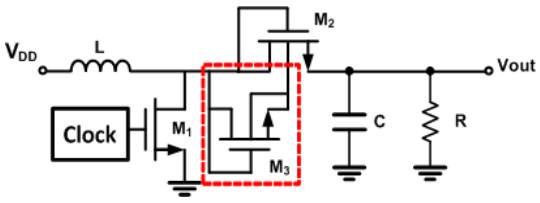


Fig. 12. Improved Boost Converter.

Fig. 14 shows signal simulation, we can see original diode-connected NMOS M_2's drain-source V_{DS}, drain-body V_{DB} and source-body V_{SB} are not exceeded 1.8 V while input voltage is 0.2 V. Thus, this harvesting system has no any component reliability problem because NMOS's any two terminals relative voltage is not too high to cause component destroyed.

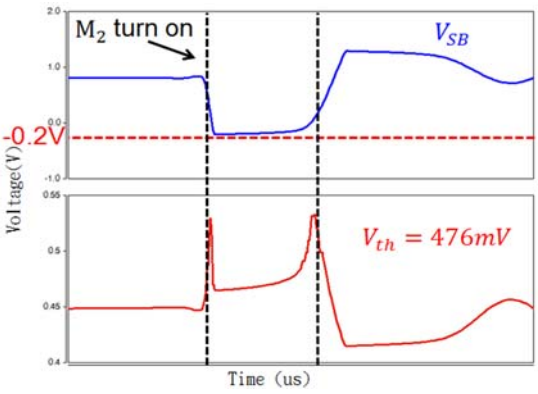


Fig. 13. Improved diode-connected NMOS's V_{th}.

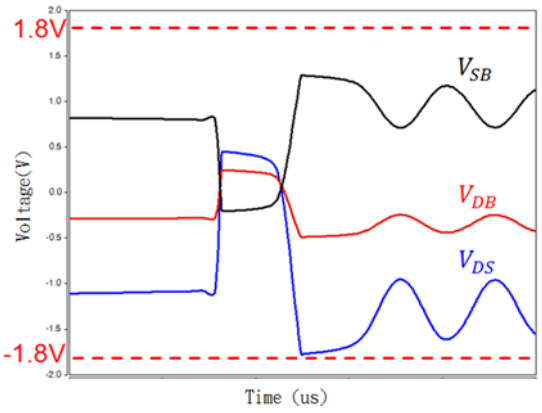


Fig. 14. Diode-connected NMOS M_2 V_{SB}, V_{DB}, V_{DS}.

3.6. Charge Control

Fig. 15 shows Charge Control. We use boost converter's output voltage as this circuit power supply. Operation shows in Fig. 16. We employ an operational amplifier (op) as a comparator to control PMOS switch. If the battery is not full charge, op will provide a high signal to turn off M_3, then current mirror turn on and copy a 300 μA current to charge the battery until the battery reach 1.2 V. When the battery's voltage is 1.2 V, op provide a low signal to make M_3 turn on. At the same time, current mirror turn off and use remained current to charge the battery. It can protect the battery to avoid overcharge that maybe damage the battery.

Next, the bandgap voltage reference circuit is composed of a BJT, six stages proportional to absolute temperature (PTAT) and a current reference circuit. So the voltage reference V_{ref} is fixed output voltage and can be insensitive to process, temperature, supply voltage. Furthermore, owing to lower V_{boost} which is only 1.3 V, current reference circuit is that cascode

three-level other than four-level in order to operate all MOS in saturation region.

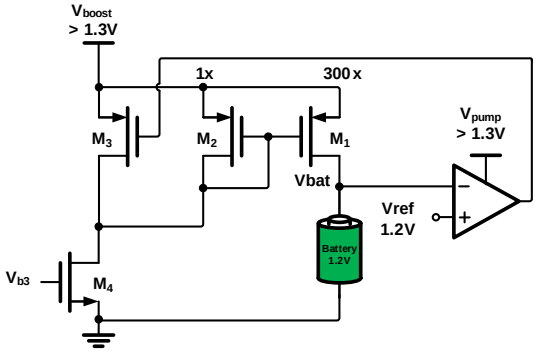


Fig. 15. Charge Control.

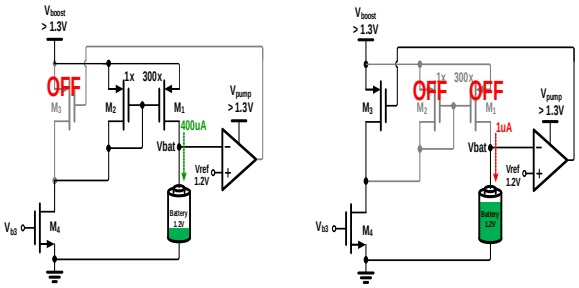


Fig. 16. Charge Control operation.

4. Experimental Results

Fig. 17 shows LC-tank measurement. As expected, it can provide a complementary clock to charge pump successfully and its amplitude achieves approximately double input voltage which range from 140~230 mV, clock frequency also has 5 MHz.

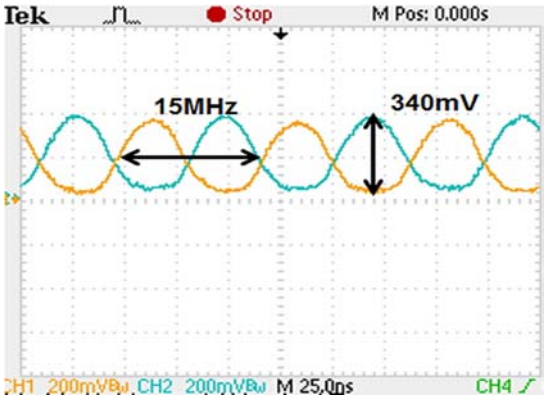


Fig. 17. LC-tank Measurement.

Fig. 18 shows Charge Pump and Duty Cycle. As usual, Charge Pump is able to boost input voltage to 500~600 mV in input voltage is from 140 mV to 230 mV, and as a stable power supply for next stage duty cycle control. Duty Cycle Control can normally produce a clock which amplitude reaches 500~600 mV and clock frequency is 5 MHz that is very important because clock signal frequency will influence next stage boost converter's boost ratio seriously.

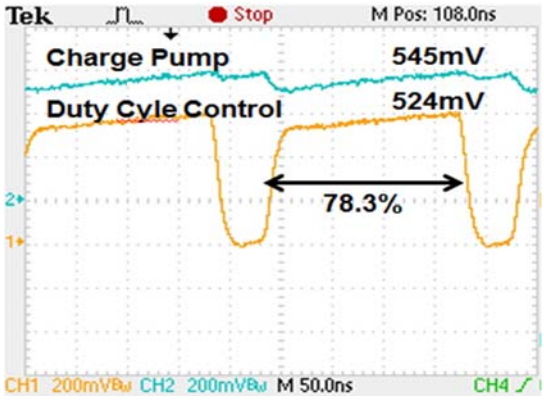


Fig. 18. Charge Pump and Duty Cycle Control Measurement.

Fig. 19 shows Boost Converter measurement in input voltage 140 mV and it can successfully boost input voltage to 1.33 V for final stage Charge Control in 57 ms later. And, its operating voltage 140 mV is minimal because we decrease input voltage under 140 mV at this time; Boost Converter's output voltage is not enough to 1.3 V that makes next stage Charge Control doesn't startup normally. Fig. 20 shows boost converter output voltage curve, you can see input voltage 0.14~0.23 V is most suitable because its output voltage is enough 1.3 V above. If input voltage is too small, its input power is not enough supply for boost converter which is not operating normally, and input voltage is too high, it will be influenced by clock's frequency. Because clock's frequency is too high, boost ratio is not as expected which can be verified by Formula (7). So boost converter also don't work normally. Finally, we test this chip's boost converter's output current in changing load, you can observe it's curve which shows in Fig. 21 correspond with ohm' law. It represents this chip is able to adjust output current in different load and provide a stable output current to load.

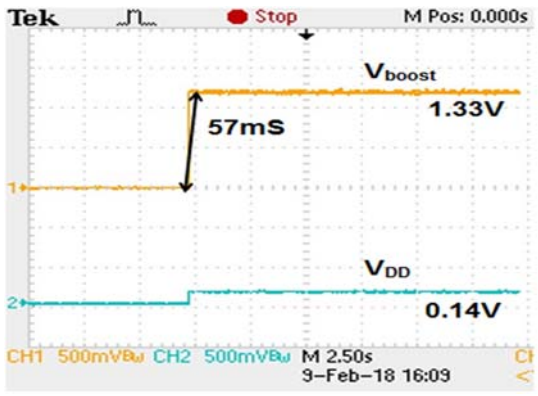


Fig. 19. Boost Converter Measurement.

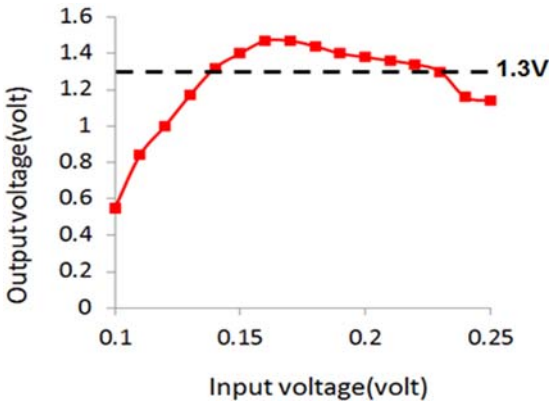


Fig. 20. Boost Converter Output Voltage Measurement.

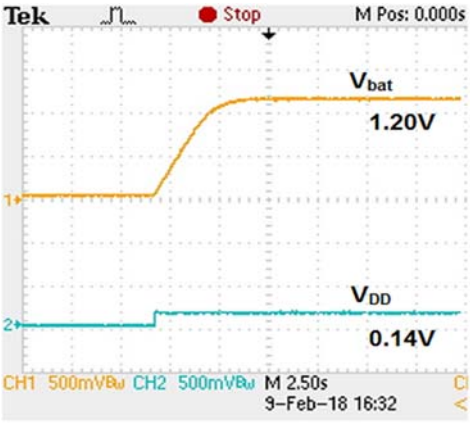


Fig. 22. Charge Control Measurement.

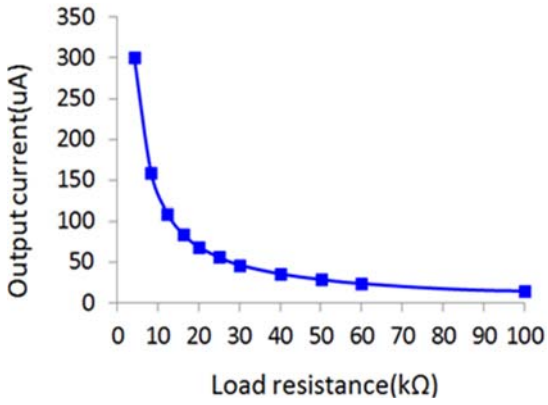


Fig. 21. Boost Converter Output Current Measurement.

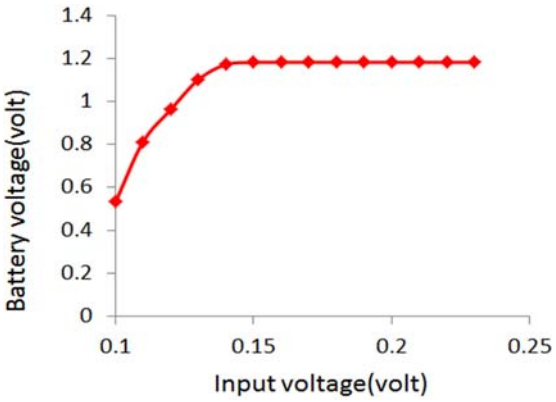


Fig. 23. NiMH battery charged voltage with input voltage.

Fig. 22 shows Charge Control measurement in input voltage 140 mV and it can successfully charge to NiMH battery to 1.2 V. Fig. 23 show NiMH battery charged voltage in different input voltage. You can observe battery voltage can be charged to 1 V when input voltage is about 0.12 V. Go on increasing input voltage to 0.14 V or higher, battery charged voltage can be successfully to 1.2 V.

Eventually, the measurement of the proposed chip is summarized in Table 1 along with state-of-the-art results from recent publications for comparison. [1-2] and [3] reference are charge pump as main boost circuit for low voltage application, and they use technology forward body biasing, backward control and dynamic body biasing respectively.

Table 1. Comparison with Low-Startup Voltage DC-DC Converter.

No.	[1]	[2]	[3]	[6]	[9]	[10]	This work
Process	65-nm CMOS	130-nm CMOS	180-nm CMOS	180-nm CMOS	CNFET	130-nm CMOS	180-nm CMOS
Min. Startup Voltage	0.18 V	0.15 V	0.32 V	0.12 V	0.10 V	0.07 V	0.12 V
Output Voltage	0.74 V @Vin=0.12 V	0.619 V @Vin=0.18 V	2.65 V @Vin=0.40 V	1.2 V @Vin=0.12 V	1.2 V @Vin=0.12 V	1.25 V @Vin=0.07 V	1.2 V @Vin=0.14 V
Output Current	7.5 uA @Vin=0.12 V	21 uA @Vin=0.18 V	3.359 uA @Vin=0.40 V	220 uA @Vin=0.12 V	120 uA @Vin=0.12 V	12 uA @Vin=0.10 V	302 uA @Vin=0.14 V
Efficiency	--	72.5 % @Vin=0.45 V	89.0 % @Vin=0.32 V	30.0 % @Vin=0.12 V	27.0 % @Vin=0.12 V	58.0 % @Vin=0.08 V	34.0 % @Vin=0.14 V
Off-chip component	None	Capacitor	Capacitor	Inductor	Inductor	PCB Inductor	Inductor Capacitor

You can observe the purposed circuit can operate in lower input voltage compare and provide a larger output to above three. Next, [6, 8, 10] are inductive type DC/DC boost converter as main boost circuit which is similar with the purposed circuit. Compared to [6] and [9], the purposed circuit can supply larger output current for next stage application and have lightly higher conversion efficiency. In [10], it can operate in lower input voltage than this work, but it uses more advanced process. Moreover, its output current is less lower than the purposed circuit. Thus, the purposed circuit will be able to be applied to a wide range of circuit compared with above reference.

5. Layout

Fig. 24 shows layout and floor plan. Core circuit is located center, and MIM capacitor is filled of main circuit above and below because it can be able to symmetry to reduce mismatch.

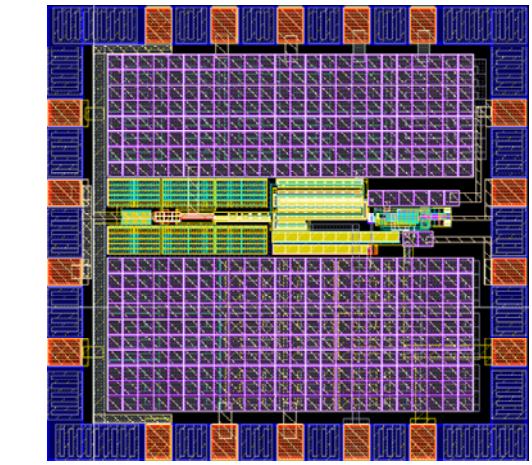


Fig. 24. Layout and Floor plan.

6. Conclusion

In this paper, the proposed harvesting system uses boost converter as a mainly boost circuit and charge pump as auxiliary circuit for startup successfully. Its operating input voltage range can be at 0.14~0.23 V and maximum conversion efficiency is about 34 %. Additionally, we use accumulation-mode MOS varactor to reduce whole chip area which can also reduce cost. In the future, the proposed harvesting system be designed a large output current 302 μA expect for objected battery, this harvesting system will be able to be applied to minimal biomedical circuit directly.

References

[1]. P. Chen, K. Ishida, X. Zhang, Y. Okuma, Y. Ryu, M. Takamiya, T. Sakurai, 0.18-V input charge pump with forward body biasing in startup circuit using 65 nm CMOS, in *Proceedings of the IEEE Custom Integrated Circuits Conf. (CICC)*, 2010, pp. 239-242.

[2]. H. Peng, N. Tang, Y. Yang, D. Heo, CMOS Startup Charge Pump with Body Bias and Backward Control for Energy Harvesting Step-Up Converters, *IEEE Trans. Circuits Syst. I*, Vol. 61, Issue 6, June 2014, pp. 1618–1628.

[3]. J. Kim, Mok, P.K.T., C. Kim, A 0.15 V Input Energy Harvesting Charge Pump with Dynamic Body Biasing and Adaptive Dead-Time for Efficiency Improvement, *IEEE Journal of Solid-State Circuits*, Vol. 50, Issue 2, Feb. 2015, pp. 414-425.

[4]. P.-H. Chen, K. Ishida, K. Ikeuchi, X. Zhang, K. Honda, Y. Okuma, Y. Ryu, M. Takamiya, T. Sakurai, A 95 mV-startup step-up converter with V^{th}-tuned oscillator by fixed-charge programming and capacitor pass-on scheme, in *Proceedings of the IEEE Int. Solid-State Conf. Dig. Tech. Papers*, 2011, pp. 216–218.

[5]. Po-Hung Chen Xin Zhang, Koichi Ishida, Yasuyuki Okuma, Yoshikatsu Ryu, Makoto Takamiya, Takayasu Sakurai, An 80 mV Startup Dual-Mode Boost Converter by Charge-Pumped Pulse Generator and Threshold Voltage Tuned Oscillator with Hot Carrier Injection, in IEEE Journal of Solid-state Circuits, Vol. 47, Issue 11, November 2012, pp. 2554-2562.

[6]. Anna Richelli, Simone Comensoli, Zsolt M. Kovács-Vajna, A DC/DC Boosting Technique and Power Management for Ultralow-Voltage Energy Harvesting Applications, in *IEEE Transactions on Industrial Electronics*, Vol. 59, Issue 6, June 2012, pp. 2701–2708.

[7]. P.-S. Weng, H.-Y. Tang, P.-C. Ku, L.-H. Lu, 50 mV-Input Batteryless Boost Converter for Thermal Energy Harvesting, in *IEEE J. Solid-State Circuits (JSSC)*, Vol. 48, Issue 4, Apr. 2013, pp. 1031–1041.

[8]. Bassi G., Colalongo L., Richelli A., Kovacs-Vajna, Z. M., 100 mV – 1.2 V fully-integrated DC – DC converters for thermal energy harvesting, *IET Power Electronics*, Vol. 6, Issue 6, July 2013, pp. 1151–1156.

[9]. Aditya Tyagi, Chalamalla Gopi, Prayank Baldi, Aminul Islam, CNFET-Based 0.1 to 1.2 V DC/DC Boost Converter with Voltage Regulation for Energy Harvesting Applications, *IEEE Trans. Circuits Syst. I*, Vol. 14, Issue 4, July 2015, pp.660–667.

[10]. Jacob Goeppert, Yiannos Manoli, Fully Integrated Startup at 70 mV of Boost Converters for Thermoelectric Energy Harvesting, in *IEEE J. Solid-State Circuits (JSSC)*, Vol. 51, July 2016, pp.1716–1726.

[11]. E. Rogers, Understanding Boost Power Stages in Switch mode Power Supplies", Application Report, Mixed Signal Products, TI Literature Number SLVA061, 1999. Online at: http://www.ti.com/lit/an/slva061/slva061.pdf.

[12]. Hong-Yi Huang, Chun-Lian Chen, Jin-Sheng Chen, Chun Yi, Kuo-Hsing Cheng, 140 mV-Startup Boost Converter for Thermal Energy Harvesting System, in *Proceedings of the 1st International Conference on Microelectronic Devices and Technologies (MicDAT'18)*, Barcelona, Spain, 20-22 June 2018, pp.110-112.

Published by International Frequency Sensor Association (IFSA) Publishing, S. L., 2018 (http://www.sensorsportal.com).



